Title

Electrophoretic and potentiometric signatures of multistage CaCO3 nucleation

Authors

Prus, Marzena

Szymanek, Karolina

Mills, Jennifer

et al.

Publication Date

2019-05-01

DOI

10.1016/j.jcis.2019.03.002

Peer reviewed

Graphical Abstract

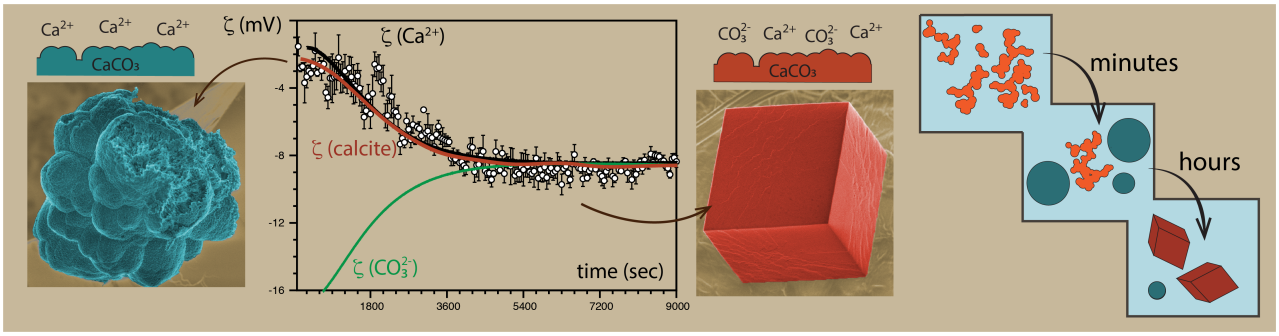

Highlights:

- time-dependent electrokinetic potential shows signatures of multistage nucleation process
- changes in ζ-potential, solution pH, saturation indexes, and particle morphology are consistent with vaterite to calcite transformation via dissolution of the former and recrystallization of the latter starting a few minutes after reagents are mixed
- ζ-potential measurements can be used to monitor polymorphic transformations of carbonate phases in-situ

Electrophoretic and Potentiometric Signatures of Multistage $CaCO_3$ Nucleation

Marzena Prus,[a] Karolina Szymanek,[b] Jennifer Mills,[c] Laura Nielsen Lammers,[c] Wojciech Piasecki,[b] Karolina Kedra-Królik,[a] Piotr Zarzycki[d,a*]

[a]Institute of Physical Chemistry, Polish Academy of Sciences, Warsaw, Poland
[b]Department of Chemistry and Biochemistry, Józef Piłsudski University of Physical Education, Warsaw, Poland
[c]Department of Environmental Science, Policy and Management, University of California, Berkeley, CA
[d]Energy Geosciences Division, Lawrence Berkeley National Laboratory, 1 Cyclotron Road, Berkeley, California, United States

Abstract

Hypothesis Calcium carbonate nucleation is often a complex and multistep process that is difficult to follow in situ. The time-resolved electrochemical and electrophoretic methods can provide a new insight into the nucleation pathway.

Experiments Here, we used a combination of speciation calculations with time-resolved electrophoretic and potentiometric methods to monitor calcium carbonate precipitation from a slightly supersaturated solution.

Findings After an initial mixing period of three minutes in which metastable $CaCO_3$ phases may have nucleated and subsequently dissolved due to locally-high supersaturations, bulk solution pH and Ca^{2+} concentrations stabilize before decreasing in tandem with the precipitation of a $CaCO_3$ phase. After an hour, the precipitate is dominated by calcite that grows at the expense of dissolving vaterite. The time-dependent electrokinetic potential shows analogous signatures of multistage nucleation process: initial rapid changes in ζ-potential are followed by much slower equilibration starting about one hour after reagents are mixed. The changes in ζ-potential, solution pH, saturation indexes, and particle morphology are consistent with vaterite to calcite transformation via dissolution of the former and recrystallization of the latter. These findings highlight the potential use of ζ-potential measurements for monitoring polymorphic transformations of carbonate phases in-situ.

*Corresponding author: e-mail: ppzarzycki@lbl.gov, Lawrence Berkeley National Laboratory M/S 74R316C, 1 Cyclotron Road, Berkeley, CA, USA, Phone: 510-486-6272

Keywords: calcium carbonate, amorphous calcium carbonate, vaterite, calcite, multistage nucleation pathway, ζ-potential, electrical double layer, carbonate speciation

1. Introduction

Calcium carbonate ($CaCO_3$) is one of the most common reactive minerals in the environment[1]; important in biomineralization[2-7], scale formation[8], and in the global carbon cycle [9, 10]. However, its crystallization is a complex process with many concurrent nucleation pathways[2, 11-36], and therefore it remains challenging to monitor in situ.

Solution saturation is the thermodynamic driving force for precipitation, and the mineral phase with the highest saturation index is expected to appear at equilibrium. However, several possible intermediate and metastable phases can precipitate first as revealed by the potentiometric[16, 18], spectroscopic[37-39], and electron/force microscopy studies[36, 40-46]. In highly supersaturated solutions, precipitation often starts via formation of amorphous calcium carbonate (ACC), which transforms directly or in stages into the thermodynamically most stable polymorph (Ostwald-Lussac rule of stages, Fig. 1a)[47]. For instance, at room temperature and in a moderate to high supersaturated solutions, the ACC transforms to calcite via vaterite as an intermediate [29] in a process that involves: dehydration and local ordering of ACC (seconds), followed by formation of vaterite (minutes) and finally its transformation to calcite (hours). However, the actual nucleation pathway is controlled by the solution composition, and it can be easily modified by impurities [29-31, 41, 48-54]. For example, Mg^{2+} ions stabilize ACC and vaterite, and as a result, they inhibit a transformation to the more stable polymorphs [29-31, 41, 50-54].

The difficulty in understanding $CaCO_3$ crystallization originates in part from the surface reactivity of growing and transforming particles – for instance, the presence of the dynamic electrical double layer (Fig. lb). For decades, sign and magnitude of surface and diffuse potential, and the identity of the potential determining ions (PDI) have been hotly debated.[34, 35, 55-64]. Now, it is broadly accepted that the constituent ions and their hydrolysis products are the primary sources of the surface charge (i.e., primary PDI) [34, 35, 65, 66]. However, the CO_2 partial pressure and bulk pH have remained important variables – as they control carbonate speciation in solution and at the surface [34, 35]. For this reason, H^+ and OH^- ions are sometimes referred to as the secondary PDI [35, 55]. Experimental insight into the surface electrostatics is frequently gained by measuring

electrokinetic potential (ζ-potential) as a function of PDI or pH. The ζ-potential is usually negative at pH >7 and it varies in magnitude among $CaCO_3$ polymorphs [34, 35, 62].

Here, we report the time-resolved electrophoretic and potentiometric monitoring of $CaCO_3$ nucleation from supersaturated solution interpreted with speciation calculations. We used a Ca-ion sensitive electrode (Ca-ISE) and pH-electrode to monitor changes in the bulk Ca^{2+} concentration and pH over time and an electrophoretic cell to follow simultaneous changes in ζ-potential. We observed signatures of multistage nucleation dynamics in the time-evolution of the aqueous composition and ζ-potential consistent with the initial precipitation of metastable vaterite that subsequently transforms into calcite via dissolution of the former and recrystallization of the latter, consistently with the previously reported sequence [29].

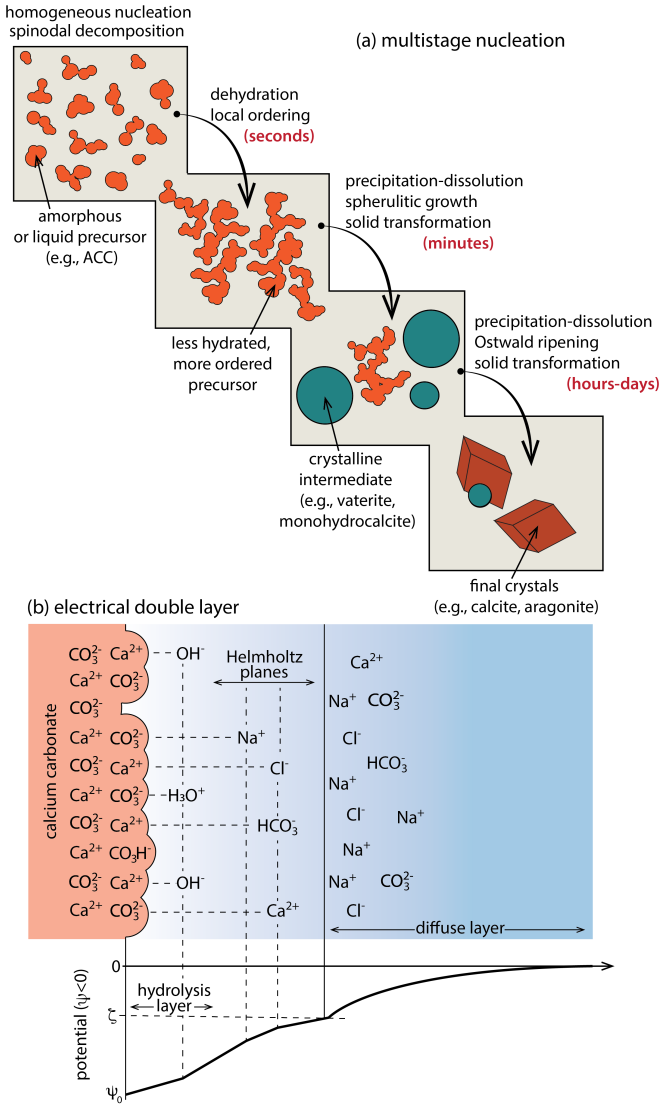

Figure 1. Schematic representation of the multistage nucleation pathway of $CaCO_3$ (a): (i) formation of amorphous calcium carbonate (ACC) or polymeric liquid precursors[2, 11-17], (ii) dehydration and local ordering[21-26] (iii) precipitation-dissolution transformation or spherulitic growth[28-33], and finally (iv) formation of the most stable $CaCO_3$ mineral. In Panel (b) we show a schematic diagram of the electrical double layer formed at the carbonate/NaCl-electrolyte interface. The surface charge is defined by constituent ions at the surface and their hydrolysis products.[34, 35] The electrokinetic potential (ζ) quantifies the electrostatic potential at the slip plane in the diffuse part of the electrical double layer.

2. Methods

2.1. Experimental Setup

In order to precipitate calcium carbonate, we mixed 2 ml of 0.1 M $CaCl_2$ (Sigma-Aldrich, pH=6) with 1 ml of 1 M NaCl, 95 ml of distilled, deionized water (Milli-Q-PLUS 185 System Polwater

CDX-100 system) and with 2 ml of 0.1 M Na_2CO_3 (Sigma-Aldrich, pH=11.4). The final volume of the solution was equal to 100 ml (2 mM effective concentration of $CaCl_2/Na_2CO_3$). This solution was prepared in the potentiometric cell (150 ml, sealed and filled with argon, Fig. S1, Supporting Information). The $CaCl_2$ solution and NaCl background electrolyte was added to the potentiometric cell first. After cell potential and pH stabilized (i.e., pH = 6), Na_2CO_3 was injected either as a single flow or as a series of two or three in the sealed cell configuration. The concentration of Ca^{2+} in the aqueous solution and bulk pH were monitored every two seconds using a calcium-selective polymer membrane electrode and a combined pH-glass/reference electrode, respectively (Metrohm, 6.0508.110, reproducibility ±4%, pH range 2-12, detection limit 5×10^{-4} mM Ca^{2+}) accompanied by reference electrode (Metrohm, 6.0750.100) and a combined pH-glass electrode with integrated Pt1000 temperature sensor, respectively (Metrohm, 6.0258.000). The Ca-ISE electrode was calibrated prior to the nucleation experiments using a 10 mM NaCl solution with varying $CaCl_2$ content. The measured concentrations of Ca^{2+} ions in the calibration step agree with the aqueous speciation calculations demonstrating that Na^+ and Cl^- ions do not interfere with the Ca-ISE (see Supporting Information). In a separate experiment, we monitor time-evolution of the ζ-potential for exactly the same experimental conditions. The ζ-potential was monitored every 50 seconds using Zetasizer Nano Z (Malvern), starting one minute after the reagents are mixed. SEM images of minerals precipitated were taken two hours after the reagents were mixed using FEI Nova NanoSEM 450. The Ca-ISE and pH-electrode response time to a change in the bulk concentration of calcium ions is less than two seconds (Fig. S2, Supporting Information).

2.2 Modeling Ions Speciation

In the seminal paper, Gebauer et al. [18] showed that Ca-ISE measurements could be instrumental in understanding the early stages of $CaCO_3$ nucleation, but their interpretation remains difficult. For instance, one cannot assume that a difference in concentration between the initially added Ca^{2+} ions and those detected by Ca-ISE is only due to (pre)nucleation of $CaCO_3$[18]; because any stable Ca^{2+} complex is also removed from the Ca-ISE-detectable pool of aqueous Ca^{2+}. To accurately interpret the Ca-ISE signal, we combined the potentiometric monitoring with speciation calculations to quantify: *i)* the amount of the precipitated solid, *ii)* aqueous phase composition, *iii)* saturation indexes of possible carbonate phases and *iv)* electrokinetic potential of precipitating particles.

We implemented a simple speciation solver to predict the distribution of aqueous species and saturation indices for possible carbonate phases considering the initial chemical composition with time-dependent pH as an input. We assume that the kinetics of ion speciation in solution is fast as compared with the nucleation process, and therefore the bulk composition equilibrates immediately with the precipitated solid. However, we do not assume that a thermodynamic equilibrium is established because the solid phase constantly evolves. Instead, we model a system far from equilibrium, assuming however, that ions complexation and speciation in the aqueous phase are rapid as compared with the rate-limiting solid-phase transformations. In our speciation calculations, we included various types of the ion pairs, because it has been suggested[67-69] that ion pairs and clusters rather than the constituent ions are the primary building blocks in carbonate crystal seeding and growth and also because Ca-ISE electrode measures only free Ca^{2+} ions in the solution – as mentioned above.

The system of nonlinear mass balance equations is modified to incorporate the additional solubility constraint and solved iteratively until the difference between the experimentally measured aqueous Ca^{2+} concentration using Ca-ISE ($c_{\mathrm{Ca}^{2+}_{aq}(exp)}$) and those calculated ($c_{\mathrm{Ca}^{2+}_{aq}(calc)}$) is less than 0.001% for a given pH value – using the amount of carbonate precipitate (Ca^{2+}_{solid}) as an optimizing variable, that is:

$$\min_{\mathrm{Ca}^{2+}_{solid}} \left(c_{\mathrm{Ca}^{2+}_{aq}(exp)} - c_{\mathrm{Ca}^{2+}_{aq}(calc)} \right) \quad (1)$$

where the amount of Ca^{2+} in solid is calculated as the difference between the total amount of Ca^{2+} (i.e., initial Ca^{2+} concentration, $c_{\mathrm{Ca}}(t_0)$) and the amount of Ca^{2+} in the aqueous phase in all possible speciation states:

$$\mathrm{Ca}^{2+}_{solid} = c_{\mathrm{Ca}}(t_0) - \sum_i^{aqueous} a_{\mathrm{Ca}_i}/\gamma_{\mathrm{Ca}_i} \quad (2)$$

where $a_{\mathrm{Ca}_i}, \gamma_{\mathrm{Ca}_i}$ are the activity and activity coefficient of Ca^{2+} in the *i*-aqueous species, respectively ($c_{\mathrm{Ca}_i} = a_{\mathrm{Ca}_i}/\gamma_{\mathrm{Ca}_i}$). All considered aqueous reactions and carbonate phases are listed in Tables 1,2. The activity coefficients were recalculated at each time-step by using the extended Debye-Hückel equation [70]:

$$\log \gamma_i = -\frac{Az_i^2\sqrt{I}}{1+Ba_i\sqrt{I}} + b_i\sqrt{I} \quad (3)$$

where A, B are the temperature dependent Debye-Hückel parameters (A=0.51, B=0.33 at T=25° C), a_i,b_i are ion-specific parameters related to the ionic radius (taken from ref.[70, 71]), z_i is the

valance of the *i*-species and *I* is the ionic strength ($I = \frac{1}{2}\sum_i z_i^2 c_i$, where c_i is the concentration of the *i*-species). The extended Debye-Hückel equation is valid for the ionic strength lower than 1 mol/dm^3 (in our system $I \leq 0.018$ mol/dm^3). The saturation index is defined for each possible *j*-carbonate phase as:

$$\mathrm{SI}_j = log \frac{a_{\mathrm{Ca}^{2+}_{aq}}\ a_{\mathrm{CO}_3^{2-}}}{K_j} \quad (4)$$

where K_j is the solubility product of a given carbonate polymorph (see Table 2).

Our speciation code was written in C++, and it uses the Newton-Raphson algorithm for the minimization procedure and iterative solver of the nonlinear equations with the compositional-constraints.

Table 1. Aqueous reactions considered in time-resolved aqueous speciation calculations.

Reaction	pK= -log$_{10}$(K)
$Ca^{2+} + Cl^- \rightleftharpoons CaCl^+$	0.696[72]
$Ca^{2+} + 2Cl^- \rightleftharpoons CaCl_{2(aq)}$	0.644[72]
$Ca^{2+} + CO_3^{2-} \rightleftharpoons CaCO^0_{3(aq)}$	-3.224[8]
$Ca^{2+} + CO_3^{2-} + H^+ \rightleftharpoons CaHCO_3^+$	-11.435[73]
$Ca^{2+} + H_2O \rightleftharpoons CaOH^+ + H^+$	12.78[73]
$Na^+ + HCO_3^- \rightleftharpoons NaHCO^0_{3(aq)}$	0.25[73]
$Na^+ + CO_3^{2-} \rightleftharpoons NaCO_3^-$	-1.27[73]
$Na^+ + OH^- \rightleftharpoons NaOH_{(aq)}$	10[73]
$Na^+ + Cl^- \rightleftharpoons NaCl_{(aq)}$	0.777[74]
$H^+ + CO_3^{2-} \rightleftharpoons HCO_3^-$	-10.329[71]
$2H^+ + CO_3^{2-} \rightleftharpoons H_2CO_{3(aq)}$	-16.681[71]

2.3. Modeling ζ-potential

There is a lack of a kinetic model of surface electrostatics (EDL) of evolving mineral particles. However the existing equilibrium models [65, 75, 76] can still shed some light on the ζ-potential behavior. Here, we use two approaches: thermodynamic Nernst-type model of surface and ζ-potential[65, 77-79] and a model based on the surface complexation approach developed by Heberling et al. [75, 76].

The thermodynamic model assumes that ion concentration at a distance *x* from the charged surface is given by the Boltzmann distribution. In the case of Ca^{2+} ions one can write:

$$[\mathrm{Ca}^{2+}]_x = [\mathrm{Ca}^{2+}]_{bulk} \exp\left(-\frac{2e\psi(x)}{k_B T}\right) \quad (5)$$

where $\psi(x)$ is the electrostatic potential at the distance x from the surface, k_B is the Boltzmann constant and T is the temperature. By rewriting eq. (5) to express ψ as a function of ionic concentrations and by considering only a specific distance that corresponds to the shear plane, we obtain the following expression for the electrokinetic potential:

$$\zeta(\mathrm{Ca^{2+}}) = \frac{k_B T}{2e} \ln \frac{[\mathrm{Ca^{2+}}]_{bulk}}{[\mathrm{Ca^{2+}}]_{IEP}} = \frac{k_B T}{2e} (p\mathrm{Ca}_{IEP} - p\mathrm{Ca}_{bulk}) \quad (6)$$

where $p\mathrm{Ca}_{IEP}$ corresponds to the particular concentration of Ca^{2+} at which $\zeta(\mathrm{Ca^{2+}}) = 0$ (i.e., isoelectric point, IEP). By analogy, a similar expression can be obtained for contribution due to the accumulation of $\mathrm{CO_3^{2-}}$ ions in the shear plane:

$$\zeta(\mathrm{CO_3^{2-}}) = \frac{k_B T}{2e} \ln \frac{[\mathrm{CO_3^{2-}}]_{IEP}}{[\mathrm{CO_3^{2-}}]_{bulk}} = \frac{k_B T}{2e} \left(p\mathrm{CO}_{3,bulk} - p\mathrm{CO}_{3,IEP}\right) \quad (7)$$

Finally, if both Ca^{2+} and $\mathrm{CO_3^{2-}}$ ions are considered as PDI, the effective electrokinetic potential can be assumed to be arithmetic or weighted average of eqs. (6,7). This derivation is inspired by Donnet et al.[65], who presented similar expressions for the surface potential of calcite and aragonite.

Although, eqs. (6,7) are convenient as they link directly aqueous composition to a measurable quantity; they do not take into account the structure of the electrical double layer formed at the mineral/electrolyte interface. To take into account surface chemistry, we used the surface complexation model as developed for calcite $(10\bar{1}4)$ crystal face/electrolyte interface by Heberling et al.[75, 76, 80] and using as input: pH, CO_3^{2-} and Ca^{2+} ions activities observed/calculated along the nucleation pathway. This approach provides the surface potential (ψ_0), which is converted to the ζ-potential by using two additional parameters a,b representing the difference in the position between the surface and slip plane and ion adsorption in Stern layer, that is [65, 67]:

$$\zeta = a\,\psi_0 + b \quad (8)$$

The eqs. (6-8), serve only as an approximation, because they are not taking into account any time-dependence of model parameters, whereas our previous studies show that EDLs vary with the type and size of the mineral particle, exposed crystal faces and surface stoichiometry [81-84].

Table 2. Solid phases considered in time-resolved aqueous speciation calculations and the initial values of the saturation index upon mixing reagents (i.e., at time t_0; allowing pH to equilibrate, but before any solid phase precipitation).

Solid phase	$pK_s = -\log_{10}(K_s)$	SI (t_0)
Calcite	8.48[73]	2.08
Aragonite	8.34[73]	1.93
Vaterite	7.91[85]	1.51
Amorphous Calcium Carbonate (ACC)	6.39[86]	-0.01
Monohydrocalcite (MHC) $CaCO_3 \times H_2O$	7.60[87]	1.20
	7.05[88]	0.65
	7.14[89]	0.74

3. Results and Discussion

In Figure S3 (Supporting Information) we show an example of the initial time-evolution of aqueous Ca^{2+} concentration and pH after $CaCl_2$ and Na_2CO_3 are mixed (time t_0) under three different Na_2CO_3 addition schemes: a) as a single flow, b) as two additions at t_0 and t_2, or c) as three additions at t_0, t_1, and t_2. All exhibit a decrease in Ca^{2+} concentration and an increase in pH with Na_2CO_3 addition; as expected, the magnitude of change in solution chemistry is proportional to the amount of Na_2CO_3 added at each time point. In all cases, Ca^{2+} concentrations rebound to higher concentrations after tens of seconds. This behavior could be interpreted to represent the precipitation and subsequent dissolution of metastable $CaCO_3$ phases or pre-nucleation clusters. However, this pattern is often observed while bulk solution chemistry is undersaturated with respect to all carbonate phases (Figure S4, Supporting Information). Thus, this behavior could either represent transient ion pairing or metastable $CaCO_3$ precipitation at locally-high supersaturation conditions during the mixing process or is simply an artifact of solution heterogeneity during the mixing process. In all cases, the calculated amount of $CaCO_3$ precipitate formed decreases to the same value as the Ca^{2+}, and pH measurements stabilize after 200s (Figure S5b, Supporting Information). We, therefore, do not further interpret any potential transient behavior during this initial mixing period and instead focus on data collected after 200 seconds. For all three additional methods, the Ca^{2+} concentration and pH stabilize to similar values (exhibiting the same Ca^{2+} drop ($\Delta c_{Ca^{2+}_{aq}}$) and pH increase (ΔpH)), so we averaged the time-evolution profiles of Ca^{2+} and bulk pH at time from t_2=70 sec to the end of experiments (9000 sec).

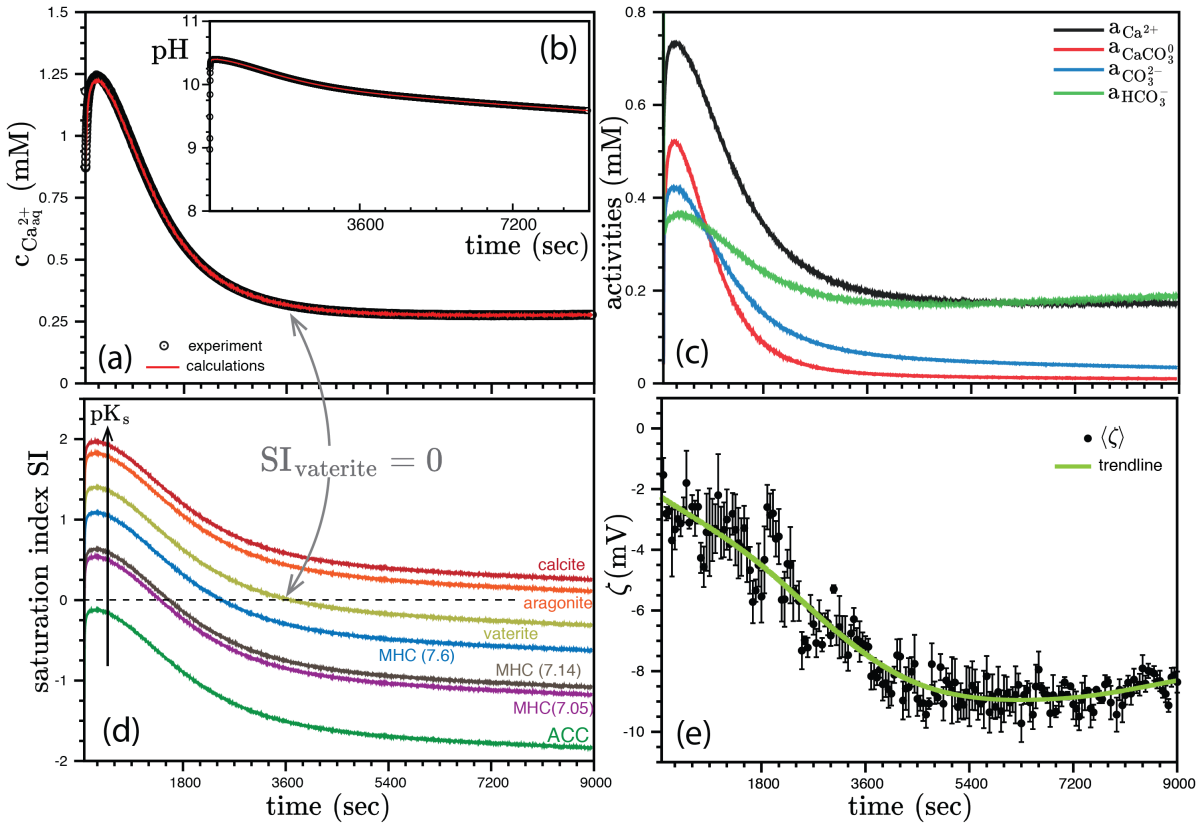

Figure 2. Comparison between experimental and calculated values of the averaged Ca^{2+} concentration and bulk pH time evolution between 70 and 9000 seconds after the reagents are mixed (a,b). In panels c,d we show the calculated evolution of aqueous speciation (c) and saturation indexes (d) obtained from the time-resolved speciation code. The electrokinetic potential (e) was obtained in a separate set of experiments using time-resolved electrophoretic cell ($\langle\zeta\rangle$=−8.62 mV after 24 hours). The green solid line illustrates the trend of the ζ-evolution and the error bars represent a standard error from three independent measurements.

In Figure 2a,b we showed the experimental and computed time evolution of bulk Ca^{2+} concentration and pH for time > 70 seconds. In the first-hour, aqueous Ca^{2+} concentration and pH decrease simultaneously, consistent with the precipitation of a $CaCO_3$ phase. After this continuous decrease, Ca^{2+} concentrations stabilize as the system approaches thermodynamic equilibrium, but interestingly the solution pH continues to decrease. SEM images taken two hours after the reagents were mixed show particles with rhombohedral morphologies – calcite, and a small number of spherulitic particles – vaterite (Fig. 3). For this reason, we propose that the nascent carbonate polymorph formed minutes after the reagents were mixed is vaterite which gradually transforms into calcite as the reaction progresses (Fig. 3a).

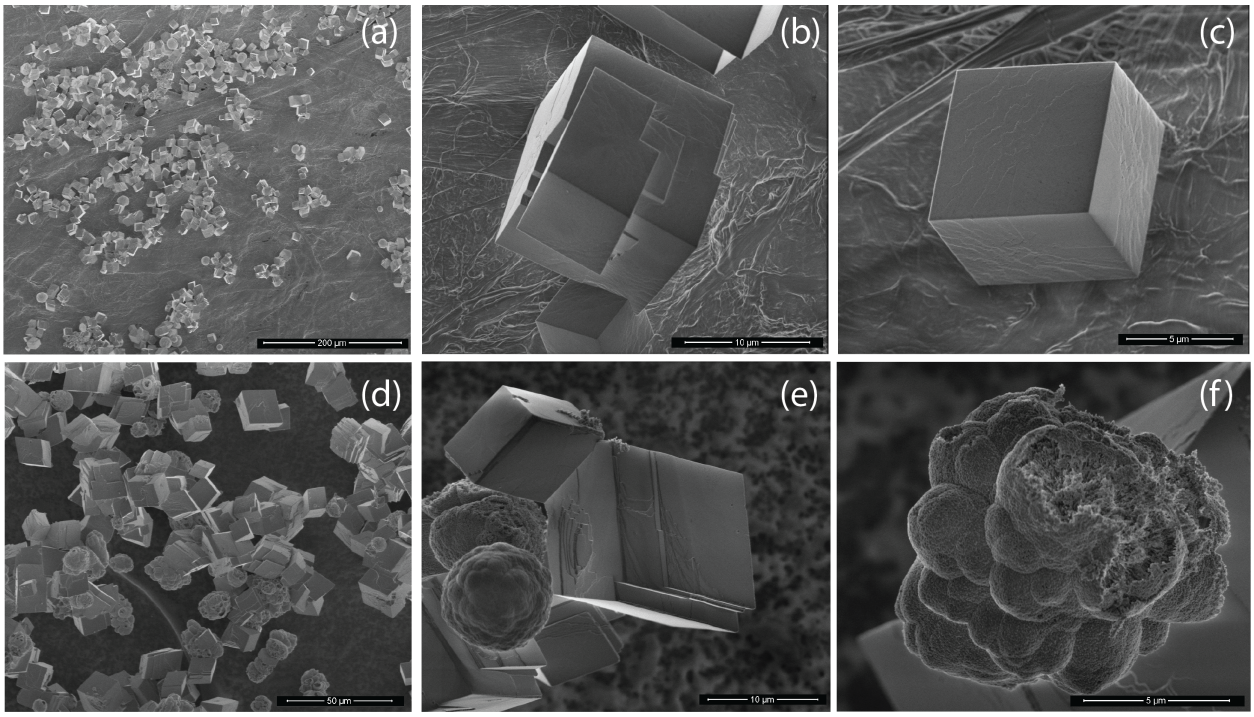

Figure 3. Scanning electron microscopy (SEM) micrographs taken two hours after the reagents were mixed and showing the presence of the calcite (rhombohedral morphology, a-c) and vaterite (spherulitic morphology, d-f) particles.

This hypothesis is supported by our calculations of saturation indexes for possible carbonate phases (Fig. 2d), which show that the stabilization of bulk Ca^{2+} concentration after one hour correlates with the solution becoming undersaturated with respect to vaterite (SI(vaterite)<0, preferential vaterite dissolution). The $SI_{calcite}$ and $SI_{aragonite}$ remain positive at t > 1 hour (Fig. 2d) – thermodynamically all vaterite particles should transform into calcite or aragonite. The latter is unlikely to precipitate in the absence of Mg^{2+} ions, consistent with the SEM images showing rhombohedral morphology typical for calcite and lack of particles with an acicular morphology characteristic of aragonite. Therefore, we conclude that the final carbonate polymorph present in the solution is calcite.

The electrokinetic potential decreases as growth progresses (from -2 mV to -8.62 mV as measured after 24 hours, Fig. 2e). The negative value of ζ-potential suggests that the particle surface is negatively charged, and it is far from being electrostatically neutralized at the slip plane. Because calcite has a lower negative ζ-potential than vaterite[35], the observed decrease of ζ-potential is again consistent with the transformation of vaterite to calcite. Moreover, the observed continued decline in solution pH after Ca^{2+} concentrations stabilize is consistent with the recrystallization of vaterite (less-negative ζ-potential, relatively more positive surface charge) to calcite (lower ζ-

potential, more negative surface charge). This transformation involves the release of H^+ from the carbonate/electrolyte interface to the solution thereby lowering bulk pH. Surface protons can be released whenever H_3O^+ near surface carbonate site/or proton from bicarbonate site is replaced by the Ca^{2+} ion, or surface Ca^{2+} ions form ion pairs with OH^- ions (see Fig. 1b):

$$\equiv CO_3^{-2}H^+ + Ca^{2+} \rightarrow \equiv CO_3^{-2}Ca^{2+} + H^+ \quad \text{or} \quad \equiv Ca^{2+} + H_2O \rightarrow \equiv Ca^{2+}OH^- + H^+ \qquad (9)$$

In Fig. 4 we show results of fitting theoretical models to observed ζ-potential profiles. The approximation offered by the Nernst-type expressions, eqs. (6,7) suggests that surface electrostatics is initially governed almost entirely by Ca^{2+} ions. The Nernst-type contribution from the carbonate ions, $\zeta(CO_3^{2-})$ becomes equal to that of Ca^{2+} ions after about one hour. This observation is consistent with changes in activities of potential determining ions in solution. Specifically, the time-evolution of Ca^{2+} resembles closely that of the ζ-potential. After one hour, the aqueous Ca^{2+} activity stabilizes, and the carbonate ions contribute equally to ζ-potential – consistently with previous studies of electrokinetic behavior of $CaCO_3$ particles [65].

The fitting based on the surface complexation modeling shows that changes in the ζ-potential reflects variations in the surface potential – this is an indication that Ca^{2+} complexation at the mineral surface is responsible for the observed consumption of Ca2+ ions from the aqoues phase and consequently for time-dependent electrokinetic behavior of transforming and growing carbonate particles.

However, the theoretical curves shown in Fig. 4 are only an approximation as they are developed for the thermodynamic equilibrium conditions. In principle, the parameters values in eqs. (6,7,8) and in the SCM model should vary in time as calcium carbonate particles evolve. At the moment, we are developing a kinetic model of EDL evolution that accompanies the particles transformation, which will be presented in the feature.

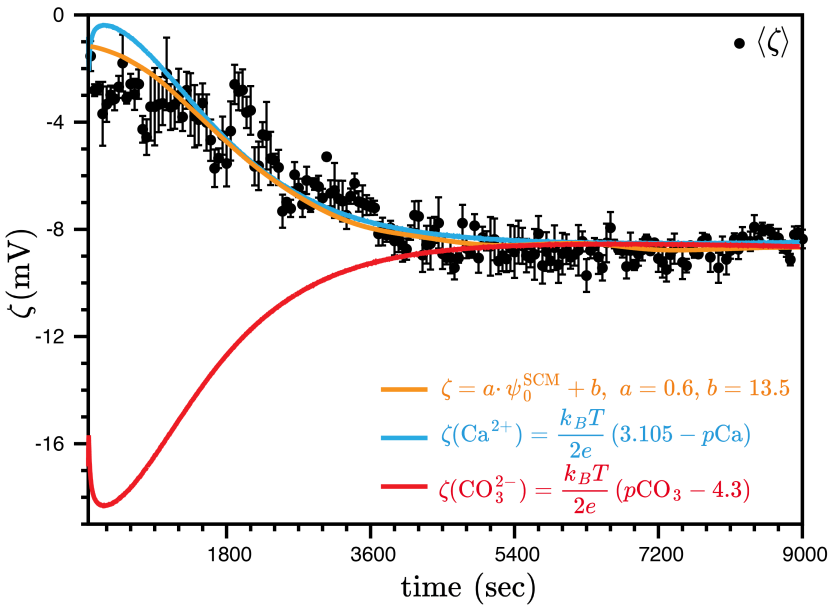

Figure 4. Measured (black dots) and calculated (solid lines, eqs. (6-8)) time-evolution of the electrokinetic potential.

5. Conclusions

The nucleation pathway of calcium carbonate is often complex and difficult to follow in situ [2, 11-36], in part due to dynamics of electrical double layer forces that governs dissolution and precipitation of carbonates [34, 35, 55-63].

By combining the speciation calculations with the time-resolved electrophoretic and potentiometric methods, we show for the first time that it is possible to monitor the evolution of the chemical composition in the aqueous phase and the electrokinetic potential developed at the precipitating/dissolving particles. Using these techniques, we monitored the precipitation of $CaCO_3$ from slightly supersaturated solution (calcium saturation index ~ 2). A metastable carbonate phase, vaterite forms within the first three minutes, and then transforms to calcite in agreement with previously reported studies [29]. After one hour, the precipitation slows as the solution approaches equilibrium with respect to calcite, but while the aqueous Ca^{2+} concentration stabilizes the solution pH continues to decline. At the same time, a dominant role of Ca^{2+} ions in determining ζ-potential decreases along with Ca^{2+} activity in the aqueous phase. We conclude that $CaCO_3$ constituent ions are the most important in governing surface electrostatics, and pH-dependent carbonate and calcium speciation is of secondary importance – in agreement with previous reports [34, 35, 64-66]. Concluding, the time-evolution of ζ-potential, solution pH, saturation indexes and particle

morphology suggest that we observe vaterite to calcite transformation within the first three hours consistent with other studies of carbonate nucleation pathways [29].

Here, we showed for the first time that a combination of the speciation calculations and time-resolved potentiometric and electrophoretic methods could provide additional insight into carbonate nucleation and growth processes, and specifically be used to identify and monitor polymorphic transformations between different carbonate phases. If these methods are combined with in-situ spectroscopic and microscopic techniques, they could provide additional insight into mineral dissolution and re-precipitation processes. What more, if such experiments are accompanied by the kinetic model of the electrical double layer of evolving particles – they will transform our understanding of relationships between surface chemistry and mineral transformation pathways.

Acknowledgment

This work was supported by the NCN Grant Sonata Bis (UMO-2016/22/E/ST4/00446). P.Z. was also supported by Laboratory Directed Research and Development (LDRD) funding from Berkeley Lab, provided by the Director, Office of Science, of the U.S. Department of Energy under Contract No. DE-AC02-05CH11231. M.P. thanks Tomasz Szymborski (IPC PAS) for assistance with the SEM imaging. P.Z. thanks Pupa Gilbert (University of Wisconsin–Madison) for helpful discussion.

References

[1] W.F. Tegethoff, Calcium Carbonate: From the Cretaceous Period Into the 21st Century, Springer, Basel, 2001.
[2] L. Addadi, S. Raz, S. Weiner, Taking Advantage of Disorder: Amorphous Calcium Carbonate and its Roles in Biomineralization, Adv Mater 15(12) (2003) 959-970.
[3] J. Aizenberg, S. Weiner, L. Addadi, Coexistence of Amorphous and Crystalline Calcium Carbonate in Skeletal Tissues, Connect Tissue Res 44 (2003) 20-25.
[4] S. Weiner, Y. Levi-Kalisman, S. Raz, L. Addadi, Biologically Formed Amorphous Calcium Carbonate, Connect Tissue Res 44 (2003) 214-218.
[5] Y. Politi, T. Arad, E. Klein, S. Weiner, L. Addadi, Sea Urchin Spine Calcite Forms via a Transient Amorphous Calcium Carbonate Phase, Science 306(5699) (2004) 1161-1164.
[6] D. Gebauer, Bio-Inspired Materials Science at Its Best-Flexible Mesocrystals of Calcite, Angew. Chem. Int. Ed. 52(32) (2013) 8208-8209.
[7] T. Mass, A.J. Giuffre, C.Y. Sun, C.A. Stifler, M.J. Frazier, M. Neder, N. Tamura, C.V. Stan, M.A. Marcus, P.U.P.A. Gilbert, Amorphous Calcium Carbonate Particles Form Coral Skeletons, P Natl Acad Sci USA 114(37) (2017) E7670-E7678.
[8] J.Y. Gal, J.C. Bollinger, H. Tolosa, N. Gache, Calcium Carbonate Solubility: A Reappraisal of Scale Formation and Inhibition, Talanta 43(9) (1996) 1497-1509.

[9] O. Hoegh-Guldberg, P.J. Mumby, A.J. Hooten, R.S. Steneck, P. Greenfield, E. Gomez, C.D. Harvell, P.F. Sale, A.J. Edwards, K. Caldeira, N. Knowlton, C.M. Eakin, R. Iglesias-Prieto, N. Muthiga, R.H. Bradbury, A. Dubi, M.E. Hatziolos, Coral Reefs Under Rapid Climate Change and Ocean Acidification, Science 318(5857) (2007) 1737-1742.
[10] E.H. Oelkers, S.R. Gislason, J. Matter, Mineral Carbonation of CO2, Elements 4(5) (2008) 333-337.
[11] M. Alberic, L. Bertinetti, Z.Y. Zou, P. Fratzl, W. Habraken, Y. Politi, The Crystallization of Amorphous Calcium Carbonate is Kinetically Governed by Ion Impurities and Water, Adv Sci 5(5) (2018) 1701000(1-9).
[12] C.R. Blue, A. Giuffre, S. Mergelsberg, N. Han, J.J. De Yoreo, P.M. Dove, Chemical and Physical Controls on the Transformation of Amorphous Calcium Carbonate into Crystalline CaCO3 Polymorphs, Geochim. Cosmochim. Acta 196 (2017) 179-196.
[13] J.H.E. Cartwright, A.G. Checa, J.D. Gale, D. Gebauer, C.I. Sainz-Diaz, Calcium Carbonate Polyamorphism and Its Role in Biomineralization: How Many Amorphous Calcium Carbonates Are There?, Angew. Chem. Int. Ed. 51(48) (2012) 11960-11970.
[14] J.J. De Yoreo, In-Situ Liquid Phase Tem Observations of Nucleation and Growth Processes, Prog Cryst Growth Ch 62(2) (2016) 69-88.
[15] J.J. De Yoreo, N.A.J.M. Sommerdijk, Investigating Materials Formation with Liquid-Phase and Cryogenic Tem, Nat Rev Mater 1(8) (2016) 1-17.
[16] D. Gebauer, H. Colfen, Prenucleation Clusters and Non-Classical Nucleation, Nano Today 6(6) (2011) 564-584.
[17] R. Demichelis, P. Raiteri, J.D. Gale, D. Quigley, D. Gebauer, Stable Prenucleation Mineral Clusters are Liquid-Like Ionic Polymers, Nat Commun 2 (2011) 590.
[18] D. Gebauer, A. Volkel, H. Colfen, Stable Prenucleation Calcium Carbonate Clusters, Science 322(5909) (2008) 1819-1822.
[19] Y. Jiang, M. Kellermeier, D. Gebauer, Z.H. Lu, R. Rosenberg, A. Moise, M. Przybylski, H. Colfen, Growth of Organic Crystals via Attachment and Transformation of Nanoscopic Precursors, Nat Commun 8 (2017) 16132.
[20] H.T. Odum, Nudibranch Spicules Made of Amorphous Calcium Carbonate, Science 114(2963) (1951) 395-395.
[21] D. Gebauer, P.N. Gunawidjaja, J.Y.P. Ko, Z. Bacsik, B. Aziz, L.J. Liu, Y.F. Hu, L. Bergstrom, C.W. Tai, T.K. Sham, M. Eden, N. Hedin, Proto-Calcite and Proto-Vaterite in Amorphous Calcium Carbonates, Angew. Chem. Int. Ed. 49(47) (2010) 8889-8891.
[22] M. Saharay, A.O. Yazaydin, R.J. Kirkpatrick, Dehydration-Induced Amorphous Phases of Calcium Carbonate, J Phys Chem B 117(12) (2013) 3328-3336.
[23] M. Saharay, R.J. Kirkpatrick, Onset of Orientational Order in Amorphous Calcium Carbonate (ACC) upon Dehydration, Chem Phys Lett 591 (2014) 287-291.
[24] M. Saharay, R.J. Kirkpatrick, Water Dynamics in Hydrated Amorphous Materials: A Molecular Dynamics Study of The Effects of Dehydration in Amorphous Calcium Carbonate, Phys Chem Chem Phys 19(43) (2017) 29594-29600.
[25] J. Ihli, W.C. Wong, E.H. Noel, Y.Y. Kim, A.N. Kulak, H.K. Christenson, M.J. Duer, F.C. Meldrum, Dehydration and Crystallization of Amorphous Calcium Carbonate in Solution and in Air, Nat Commun 5(3169) (2014) 1-10.
[26] M. Farhadi-Khouzani, D.M. Chevrier, P. Zhang, N. Hedin, D. Gebauer, Water as the Key to Proto-Aragonite Amorphous $CaCO_3$, Angew. Chem. Int. Ed. 55(28) (2016) 8117-8120.

[27] K. Kedra-Krolik, P. Gierycz, Simulation of Nucleation and Growing of CaCO3 Nanoparticles Obtained in The Rotating Disk Reactor, J. Cryst. Growth 312(12-13) (2010) 1945-1951.
[28] F.F. Amos, D.M. Sharbaugh, D.R. Talham, L.B. Gower, M. Fricke, D. Volkmer, Formation of Single-Crystalline Aragonite Tablets/Films via an Amorphous Precursor, Langmuir 23(4) (2007) 1988-1994.
[29] P. Bots, L.G. Benning, J.D. Rodriguez-Blanco, T. Roncal-Herrero, S. Shaw, Mechanistic Insights into the Crystallization of Amorphous Calcium Carbonate (ACC), Cryst. Growth Des. 12(7) (2012) 3806-3814.
[30] J.D. Rodriguez-Blanco, S. Shaw, P. Bots, T. Roncal-Herrero, L.G. Benning, The Role of Mg in the Crystallization of Monohydrocalcite, Geochim. Cosmochim. Acta 127 (2014) 204-220.
[31] J.D. Rodriguez-Blanco, S. Shaw, P. Bots, T. Roncal-Herrero, L.G. Benning, The Role of pH and Mg on the Stability and Crystallization of Amorphous Calcium Carbonate, J Alloy Compd 536 (2012) S477-S479.
[32] J.W. Singer, A.O. Yazaydin, R.J. Kirkpatrick, G.M. Bowers, Structure and Transformation of Amorphous Calcium Carbonate: A Solid-State Ca-43 NMR and Computational Molecular Dynamics Investigation, Chem Mater 24(10) (2012) 1828-1836.
[33] J.M. Walker, B. Marzec, F. Nudelman, Solid-State Transformation of Amorphous Calcium Carbonate to Aragonite Captured by CryoTEM, Angew. Chem. Int. Ed. 56(39) (2017) 11740-11743.
[34] D. Al Mahrouqi, J. Vinogradov, M.D. Jackson, Zeta Potential of Artificial and Natural Calcite in Aqueous Solution, Adv Colloid Interfac 240 (2017) 60-76.
[35] I. Sondi, J. Biscan, N. Vdovic, S.D. Skapin, The Electrokinetic Properties of Carbonates in Aqueous Media Revisited, Colloid Surface A 342(1-3) (2009) 84-91.
[36] M.H. Nielsen, S. Aloni, J.J. De Yoreo, In situ TEM imaging of CaCO3 nucleation reveals coexistence of direct and indirect pathways, Science 345(6201) (2014) 1158-1162.
[37] F. Sebastiani, S.L. Wolf, B. Born, T.Q. Luong, H. Colfen, D. Gebauer, M. Havenith, Water Dynamics from THz Spectroscopy Reveal the Locus of a Liquid-Liquid Binodal Limit in Aqueous CaCO3 Solutions, Angew Chem Int Ed Engl 56(2) (2017) 490-495.
[38] J.R.I. Lee, T.Y.J. Han, T.M. Willey, D. Wang, R.W. Meulenberg, J. Nilsson, P.M. Dove, L.J. Terminello, T. van Buuren, J.J. De Yoreo, Structural development of mercaptophenol self-assembled monolayers and the overlying mineral phase during templated CaCO3 crystallization from a transient amorphous film, J. Am. Chem. Soc. 129(34) (2007) 10370-10381.
[39] M.H. Nielsen, J.R.I. Lee, Q.N. Hu, T.Y.J. Han, J.J. De Yoreo, Structural evolution, formation pathways and energetic controls during template-directed nucleation of CaCO3, Faraday Discuss 159 (2012) 105-121.
[40] H.H. Teng, P.M. Dove, C.A. Orme, J.J. De Yoreo, Thermodynamics of calcite growth: Baseline for understanding biomineral formation, Science 282(5389) (1998) 724-727.
[41] K.J. Davis, P.M. Dove, J.J. De Yoreo, The role of Mg2+ as an impurity in calcite growth, Science 290(5494) (2000) 1134-1137.
[42] H.H. Teng, P.M. Dove, J.J. De Yoreo, Kinetics of calcite growth: Surface processes and relationships to macroscopic rate laws, Geochim. Cosmochim. Acta 64(13) (2000) 2255-2266.
[43] M.H. Nielsen, D.S. Li, H.Z. Zhang, S. Aloni, T.Y.J. Han, C. Frandsen, J. Seto, J.F. Banfield, H. Colfen, J.J. De Yoreo, Investigating Processes of Nanocrystal Formation and Transformation via Liquid Cell TEM, Microsc Microanal 20(2) (2014) 425-436.
[44] P.J.M. Smeets, K.R. Cho, R.G.E. Kempen, N.A.J.M. Sommerdijk, J.J. De Yoreo, Calcium carbonate nucleation driven by ion binding in a biomimetic matrix revealed by in situ electron microscopy, Nat Mater 14(4) (2015) 394-399.

[45] P.J.M. Smeets, D. Li, M.H. Nielsen, K.R. Cho, N.A.J.M. Sommerdijk, J.J. De Yoreo, Unraveling the CaCO3 Mesocrystal Formation Mechanism Including a Polyelectrolyte Additive using in-situ TEM and in-situ AFM, Adv Imag Elect Phys 179 (2013) 165-167.
[46] A.F. Wallace, L.O. Hedges, A. Fernandez-Martinez, P. Raiteri, J.D. Gale, G.A. Waychunas, S. Whitelam, J.F. Banfield, J.J. De Yoreo, Microscopic Evidence for Liquid-Liquid Separation in Supersaturated CaCO3 Solutions, Science 341(6148) (2013) 885-889.
[47] S. Leukel, M. Panthöfer, M. Mondeshki, G. Kieslich, Y. Wu, N. Krautwurst, W. Tremel, Trapping Amorphous Intermediates of Carbonates – A Combined Total Scattering and NMR Study, J. Am. Chem. Soc. 140 (2018) 14638−14646.
[48] Y.W. Wang, Y.Y. Kim, C.J. Stephens, F.C. Meldrum, H.K. Christenson, In Situ Study of the Precipitation and Crystallization of Amorphous Calcium Carbonate (ACC), Cryst. Growth Des. 12(3) (2012) 1212-1217.
[49] P.M. Dove, L.E. Wasylenki, D.S. Wilson, J.J. De Yoreo, Kinetics and thermodynamics of Sr and Mg interactions with calcite during growth: Deciphering mineralization processes, Geochim. Cosmochim. Acta 68(11) (2004) A200-A200.
[50] B. Purgstaller, F. Konrad, M. Dietzel, A. Immenhauser, V. Mavromatis, Control of Mg2+/Ca2+ Activity Ratio on the Formation of Crystalline Carbonate Minerals via an Amorphous Precursor, Cryst. Growth Des. 17(3) (2017) 1069-1078.
[51] E. Loste, R.M. Wilson, R. Seshadri, F.C. Meldrum, The role of magnesium in stabilising amorphous calcium carbonate and controlling calcite morphologies, J. Cryst. Growth 254(1-2) (2003) 206-218.
[52] J.K. Berg, T. Jordan, Y. Binder, H.G. Borner, D. Gebauer, Mg2+ Tunes the Wettability of Liquid Precursors of CaCO3: Toward Controlling Mineralization Sites in Hybrid Materials, J. Am. Chem. Soc. 135(34) (2013) 12512-12515.
[53] A. Koishi, A. Fernandez-Martinez, B. Ruta, M. Jimenez-Ruiz, R. Poloni, A. di Tommaso, F. Zontone, G.A. Waychunas, G. Montes-Hernandez, Role of Impurities in the Kinetic Persistence of Amorphous Calcium Carbonate: A Nanoscopic Dynamics View, J Phys Chem C 122(29) (2018) 16983-16991.
[54] Z.N. Zhang, Y.D. Xie, X.R. Xu, H.H. Pan, R.K. Tang, Transformation of amorphous calcium carbonate into aragonite, J. Cryst. Growth 343(1) (2012) 62-67.
[55] P. Somasundaran, G.E. Agar, Zero Point of Charge of Calcite, J. Colloid Interface Sci. 24(4) (1967) 433-440.
[56] T. Foxall, G.C. Peterson, H.M. Rendall, A.L. Smith, Charge Determination at Calcium Salt Aqueous Solution Interface, J Chem Soc Farad T 1 75 (1979) 1035-1039.
[57] B. Siffert, P. Fimbel, Parameters Affecting the Sign and the Magnitude of the Electrokinetic Potential of Calcite, Colloid Surface 11(3-4) (1984) 377-389.
[58] Y.C. Huang, F.M. Fowkes, T.B. Lloyd, N.D. Sanders, Adsorption of Calcium-Ions from Calcium-Chloride Solutions onto Calcium-Carbonate Particles, Langmuir 7(8) (1991) 1742-1748.
[59] E. Chibowski, L. Holysz, W. Wojcik, Changes in Zeta-Potential and Surface Free-Energy of Calcium-Carbonate Due to Exposure to Radiofrequency Electric-Field, Colloid Surface A 92(1-2) (1994) 79-85.
[60] E. Chibowski, L. Hotysz, A. Szczes, Time dependent changes in zeta potential of freshly precipitated calcium carbonate, Colloid Surface A 222(1-3) (2003) 41-54.
[61] L. Holysz, M. Chibowski, E. Chibowski, Time-dependent changes of zeta potential and other parameters of in situ calcium carbonate due to magnetic field treatment, Colloid Surface A 208(1-3) (2002) 231-240.

[62] C. Xu, C. Walsh, E. Boaretto, K.M. Poduska, Assessing the feasibility of electrophoretic separation of CaCO3 polymorphs for archaeological applications, Anal Methods-Uk 9(3) (2017) 427-433.
[63] J.J. Predali, J.M. Cases, Zeta Potential of Magnesian Carbonates in Inorganic Electrolytes, J. Colloid Interface Sci. 45(3) (1973) 449-458.
[64] D.W. Thompson, P.G. Pownall, Surface Electrical-Properties of Calcite, J. Colloid Interface Sci. 131(1) (1989) 74-82.
[65] M. Donnet, P. Bowen, J. Lemaitre, A thermodynamic solution model for calcium carbonate: Towards an understanding of multi-equilibria precipitation pathways, J. Colloid Interface Sci. 340(2) (2009) 218-224.
[66] N. Vdovic, D. Kralj, Electrokinetic properties of spontaneously precipitated calcium carbonate polymorphs: the influence of organic substances, Colloid Surface A 161(3) (2000) 499-505.
[67] E. Ruiz-Agudo, C.V. Putnis, C. Rodriguez-Navarro, A. Putnis, Effect of pH on calcite growth at constant a(Ca2+)/a(CO32-) ratio and supersaturation, Geochim. Cosmochim. Acta 75(1) (2011) 284-296.
[68] O. Nilsson, J. Sternbeck, A mechanistic model for calcite crystal growth using surface speciation, Geochim. Cosmochim. Acta 63(2) (1999) 217-225.
[69] A. Carino, A. Testino, M.R. Andalibi, F. Pilger, P. Bowen, C. Ludwig, Thermodynamic-Kinetic Precipitation Modeling. A Case Study: The Amorphous Calcium Carbonate (ACC) Precipitation Pathway Unravelled, Cryst. Growth Des. 17(4) (2017) 2006-2015.
[70] D.L. Parkhurst, Ion-Association Models and Mean Activity-Coefficients of Various Salts, Acs Sym Ser 416 (1990) 30-43.
[71] C.A.J. Appelo, D.L. Parkhurst, V.E.A. Post, Equations for calculating hydrogeochemical reactions of minerals and gases such as CO2 at high pressures and temperatures, Geochim. Cosmochim. Acta 125 (2014) 49-67.
[72] M. Neveu, S.J. Desch, J.C. Castillo-Rogez, Aqueous geochemistry in icy world interiors: Equilibrium fluid, rock, and gas compositions, and fate of antifreezes and radionuclides, Geochim. Cosmochim. Acta 212 (2017) 324-371.
[73] S.R. Charlton, D.L. Parkhurst, Modules based on the geochemical model PHREEQC for use in scripting and programming languages, Comput Geosci-Uk 37(10) (2011) 1653-1663.
[74] J.A. Johnson, F. Anderson, D.L. Parkhurst, Database thermo.com.V8.R6.230, in: L.L.N. Laboratory (Ed.) Lawrence Livermore National Laboratory, Livermore CA, 2000.
[75] F. Heberling, T.P. Trainor, J. Lutzenkirchen, P. Eng, M.A. Denecke, D. Bosbach, Structure and Reactivity of the Calcite-Water Interface, J. Colloid Interface Sci. 354(2) (2011) 843-857.
[76] F. Heberling, D. Bosbach, J.D. Eckhardt, U. Fischer, J. Glowacky, M. Haist, U. Kramar, S. Loos, H.S. Muller, T. Neumann, C. Pust, T. Schafer, J. Stelling, M. Ukrainczyk, V. Vinograd, M. Vucak, B. Winkler, Reactivity of the Calcite-Water-Interface, From Molecular Scale Processes to Geochemical Engineering, Appl Geochem 45 (2014) 158-190.
[77] P. Zarzycki, Comparison of the Monte Carlo Estimation of Surface Electrostatic Potential at the Hematite (0001)/Electrolyte Interface with the Experiment, Appl Surf Sci 253(18) (2007) 7604-7612.
[78] P. Zarzycki, K.M. Rosso, Nonlinear Response of the Surface Electrostatic Potential Formed at Metal Oxide/Electrolyte Interfaces. A Monte Carlo Simulation Study, J. Colloid Interface Sci. 341(1) (2010) 143-152.

[79] P. Zarzycki, K.M. Rosso, S. Chatman, T. Preocanin, N. Kallay, W. Piasecki, Theory, Experiment and Computer Simulation of the Electrostatic Potential at Crystal/Electrolyte Interfaces, Croat Chem Acta 83(4) (2010) 457-474.
[80] F. Heberling, T.P. Trainor, J. Lutzenkirchen, P. Eng, M.A. Denecke, D. Bosbach, Structure and Reactivity of the Calcite-Water Interface (vol 354, pg 843, 2011), J. Colloid Interface Sci. 404 (2013) 230-230.
[81] P. Zarzycki, T. Preocanin, Point of Zero Potential of Single-Crystal Electrode/Inert Electrolyte Interface, J. Colloid Interface Sci. 370 (2012) 139-143.
[82] P. Zarzycki, S. Chatman, T. Preocanin, K.M. Rosso, Electrostatic Potential of Specific Mineral Faces, Langmuir 27(13) (2011) 7986-7990.
[83] K. Kedra-Krolik, K.M. Rosso, P. Zarzycki, Probing Size-Dependent Electrokinetics of Hematite Aggregates, J. Colloid Interface Sci. 488 (2017) 218-224.
[84] S. Chatman, P. Zarzycki, K.M. Rosso, Surface Potentials of (001), (012), (113) Hematite (alpha-Fe2o3) Crystal Faces in Aqueous Solution, Phys Chem Chem Phys 15(33) (2013) 13911-13921.
[85] E. Giffaut, M. Grive, P. Blanc, P. Vieillard, E. Colas, H. Gailhanou, S. Gaboreau, N. Marty, B. Made, L. Duro, Andra thermodynamic database for performance assessment: ThermoChimie, Appl Geochem 49 (2014) 225-236.
[86] L. Brecevic, A.E. Nielsen, Solubility of Amorphous Calcium-Carbonate, J. Cryst. Growth 98(3) (1989) 504-510.
[87] H. Hull, A.G. Turnbull, Thermochemical Study of Monohydrocalcite, Geochim. Cosmochim. Acta 37(3) (1973) 685-694.
[88] D. Kralj, L. Brecevic, Dissolution Kinetics and Solubility of Calcium-Carbonate Monohydrate, Colloid Surface A 96(3) (1995) 287-293.
[89] J.D. Allison, D.S. Brown, K.J. Novo-Gradac, MINTEQA2/ProdefA2, A Geochemical Assessment Model for Environmental Systems, 1991.